Research Square

Preprints are preliminary reports that have not undergone peer review.
They should not be considered conclusive, used to inform clinical practice,
or referenced by the media as validated information.

Bentonite as a low-cost binder for mesoporous aluminosilicate composites: toward sustainable and cost-effective materials

Kamilla Umbetkaliyeva
Farabi University
Mariya Shayakhmetova
Almaty Technological University
Tleutai Abildin
Farabi University
Fatima Kanapiyeva
Farabi University
Dilara Bagu
Farabi University
Saule Akhmetova
Almaty Technological University
Gulzira Vassilina
vasilinagulzira@gmail.com

Almaty Technological University

Article

Keywords: bentonite, mesoporous aluminosilicate, catalyst support, low-cost binder, acid activation, mechanical strength, cost-efficiency, sustainable materials

Posted Date: August 31st, 2026

DOI: https://doi.org/10.21203/rs.3.rs-10697778/v1

License: This work is licensed under a Creative Commons Attribution 4.0 International License. Read Full License

Additional Declarations: No competing interests reported.

Abstract

Acid-activated bentonite from the Tagan field (Kazakhstan) was investigated as a low-cost binder for mesoporous aluminosilicate (MAS) composites. The mineralogical, acidic, textural, thermal, and mechanical properties of the materials were studied together with an assessment of material cost. H-bentonite showed a high concentration of weak acid sites (4819 μmol NH_3/g), while its incorporation into MAS preserved the mesoporous structure. The composite containing 35 wt.% H-bentonite had a specific surface area of 375.1 m²/g and an average pore diameter of 3.5 nm, while its mechanical strength in-creased from 27.1 to 30.2 kg/cm². Partial replacement of synthetic MAS with bentonite reduced the calculated material cost by approximately 56% at a MAS ratio of 35:65 and by 69% at 20:80. These results demonstrate that locally available Tagan bentonite can serve as an effective low-cost binder for mesoporous aluminosilicate composites, reducing the use of expensive synthetic components while maintaining the properties required for catalyst-support applications.

1. Introduction

The development of industrial technologies is leading to a steady expansion in the applications of natural clay minerals. This is particularly true for minerals of the smectite group, primarily bentonite clays, whose main component is montmorillonite. Montmorillonite is one of the most common minerals in soils, the primary component of bentonite clays, and is found in many sedimentary rocks [1]. Bentonites belong to the class of layered clay-type silicates, the common properties of which are dispersibility, colloidality, swellability, and adsorption. They possess high binding capacity, ion-exchange, absorption, and bleaching properties, as well as low cost and wide availability, which allows for their effective use in solving complex environmental problems [2].

Bentonite, a smectite-rich sedimentary rock primarily composed of montmorillonite, is characterized by a unique 2:1 layered aluminosilicate structure where an octahedral alumina sheet is sandwiched between two tetrahedral silica sheets [3–7].

Metal cations (Na^+, Ca^{2+}, K^+, Mg^{2+}, less commonly Li^+, and sometimes the NH_4^+ group) are located in the interlayer space of montmorillonite. They balance the negative charges of the layers. Most often, all the cations listed above are present in the exchange complex. One of the properties of montmorillonite clays is the possibility of their activation and modification (loosening the sorbent microstructure) using various methods, which is aimed at increasing porosity and specific surface area, enhancing ion-exchange properties, and creating various active centers [8–10].

This configuration, coupled with isomorphic substitutions within the crystal lattice, results in a net negative surface charge neutralized by exchangeable cations (Na^+, Ca^{2+}, Mg^{2+}) and hydrated layers within the interlayer galleries [3, 4, 11–14]. These structural features endow the material with an exceptional cation exchange capacity (CEC), a high specific surface area, and remarkable swelling potential [15–17]. Such intrinsic properties facilitate its widespread deployment in critical engineering applications, most notably as engineered barriers (e.g., MX-80 and GMZ grades) in high-level radioactive waste repositories due to its low permeability and radionuclide retention capabilities [15, 18–19]. Furthermore, its robust binding properties and cost-effectiveness position it as a standard binder in iron ore pelletization and as a structural stabilizer in composite catalyst supports, where its efficiency is fundamentally modulated by process water chemistry and ion exchange dynamics [20].

To broaden its functional scope, targeted modifications are extensively employed. Acid activation (typically utilizing H_2SO_4 or HCl) leaches octahedral cations to produce a nanoporous silica-rich framework with increased surface acidity, optimizing the clay for heterogeneous catalysis and bleaching applications [21–22]. Concurrently, pillaring with metal polycations (e.g., Al, Fe, Zn, Zr) serves to fix the interlayer distance, preventing structural collapse and creating thermally stable active centers suitable for Friedel-Crafts alkylation [4, 21, 23–24]. Modern material design further integrates organic functionalization through surfactant intercalation (e.g., HDTMA, CTAB) or hybridization with polymers such as polyacrylamide, microcrystalline cellulose, and chitosan [6, 25]. These modifications transform the hydrophilic clay surface into a highly selective organophilic or multidentate coordination interface, exhibiting superior performance in the removal of recalcitrant pollutants, including methylene blue dye, phenolic compounds, and heavy metals (Pb^{2+}, Cu^{2+}, Cd^{2+}), from complex wastewater matrices [17]. Finally, emerging research underscores the potential of bentonite as a pozzolanic supplementary cementitious material for sustainable concrete and as a support for bismuth oxide in gamma radiation shielding materials [26]. Consequently, the synergy between intrinsic structural flexibility and the capacity for targeted physicochemical modulation positions bentonite as a cornerstone material for the development of high-performance adsorbents, catalyst supports, and next-generation protective materials.

Thanks to this unique combination of properties, bentonite clays are used in nearly all key industrial sectors—from oil and gas drilling and metallurgy to construction, agriculture, and environmental protection—which drives the steady growth in global demand for this raw material. According to the U.S. Geological Survey, global bentonite production in 2025 was approximately 20 million tons (19.4 million tons in 2024), with the leading producing countries including the USA, India, China, and Turkey [27].

Against this backdrop, the development of the bentonite industry in countries with their own, but not fully exploited, resource base is of natural interest. Kazakhstan is one such country, possessing significant explored deposits of bentonite clays, including the largest ones: Sarbai, Tagan, Dinozavrovoye, Akzhar, Keles, etc. [2]. According to the Bureau of National Statistics of the Agency for Strategic Planning and Reforms of the Republic of Kazakhstan, the country's bentonite production volume (see Fig. 1) shows pronounced volatility over the 2010–2025 period: from 12 thousand tons in 2010 to a peak of 358 thousand tons in 2015, followed by stabilization at 44–106 thousand tons between 2017 and 2025 (76.5 thousand tons in 2025) [28]. These trends indicate significant unrealized potential in the industry amid a steady rise in global demand.

The oil refining industry is one of the promising areas for expanding the industrial application of Kazakhstani bentonite. This is partly due to large-scale plans to modernize this sector: according to the Concept for the Development of the Oil Refining Industry of the Republic of Kazakhstan for 2025–2040, the country plans to more than double its refining capacity by 2040 – from 18 to 39 million tons of oil per year [29]. This implies a proportional increase in demand for the auxiliary materials and catalyst systems used in oil refining processes. Currently, however, the catalyst systems used by Kazakhstan's oil refineries are primarily imported, which creates additional industry dependence on foreign suppliers and highlights the need to develop domestic alternatives based on available local raw materials.

In this context, the use of modified bentonite as a catalyst support component for oil refining processes is of particular interest. This area was previously investigated by the authors of this paper [30–33], where the main focus was on the catalytic activity of the developed system and the characteristics of the first key support component—mesoporous aluminosilicate. In the present work, the research focus shifts to the second key component of the composite support—bentonite clay from the Tagan field, which serves as a low-cost binder. Its role is considered from the perspective of sustainable development, both in terms of reducing costs and increasing the availability of raw materials, and in light of the environmental advantages of its use compared to alternative binding materials.

The objective of this study is to investigate the influence of bentonite content, as a binding component, on the physicochemical/structural characteristics of composites based on mesoporous aluminosilicates and to evaluate the economic efficiency of its use.

2. Methods

Mesostructured aluminosilicates (MAS-1 and MAS-2) with a high aluminum content were synthesized by the co-condensation of tetraethyl orthosilicate, $Si(OC_2H_5)_4$, and aluminum sources—aluminum isopropoxide, $Al(O\text{-}i\text{-}Pr)_3$ (for MAS-1), and aluminum sec-butoxide, $(sec\text{-}BuO)_3Al$ (for MAS-2). In this method, hexadecylamine was used as a structure-directing template. The composite supports MAS-1-H-bentonite and MAS-2-H-bentonite were prepared by mechanically mixing the synthesized MAS-1 and MAS-2 (from each of the two aluminum precursors) with H-bentonite in MAS (1 or 2): H-bentonite mass ratios of 20:80 and 35:65, followed by extrusion, drying, and calcination. A detailed synthesis methodology is provided in the authors' previously published works [30–33].

The phase composition of the bentonite was determined by X-ray diffraction (XRD) analysis. Diffractograms were recorded on a DRON-4 diffractometer using CuKα radiation at a tube voltage of 30 kV and a current of 30 mA. The detector scanning speed was 2 and 0.5 degrees per minute. For quantitative phase analysis, diffractograms were recorded with the sample rotating around a horizontal axis. To prevent oxidation, the catalyst samples, after being washed with water and absolute methanol, were mixed with BF-2 adhesive. This mixture was placed in an ebonite sample holder 20 mm in diameter and 0.5 mm deep. After drying at room temperature, the sample surface was polished with fine sandpaper.

The chemical composition of bentonite was determined by X-ray fluorescence (XRF) and X-ray photoelectron spectroscopy (XPS). The procedure involves exciting the X-ray fluorescence of the elements in the sample using mixed primary radiation from an X-ray tube with a silver anode. The intensity of the fluorescent Kα lines of the target compounds was measured using an ARF-6 X-ray fluorescence analyzer, equipped with a silver anode X-ray tube.

Temperature-programmed desorption of ammonia (NH3-TPD) was performed on a USGA-101 unit. A sample weighing 0.1 g (0.30–0.50 mm fraction) was placed in a quartz reactor, calcined at 512°C in a helium flow (139 min, 20 ml/min), and then cooled. Adsorption of ammonia (7 vol.% NH_3 in N_2, flow rate of 40 ml/min) was carried out at 102°C for 1 h, after which the system was purged with helium (60 min). The TPD curves were recorded in a helium flow (8 ml/min) from 60 to 600°C at a linear heating rate of 8°C/min.

The porous structure of the synthesized samples and their BET surface area values were studied using the standard nitrogen adsorption/desorption method on a QuantaChrome Autosorb-6 sorptometer. Before the analysis, the samples were evacuated at 300°C for 12 hours to a pressure of $3x10^{-3}$ atm. The nitrogen adsorption-desorption isotherm was recorded at a temperature of 77 K. The porous structure characteristics were calculated using standard software. The specific surface area was calculated using the BET (Brunauer-Emmett-Teller) model at a relative partial pressure of $P/P_0 = 0.2$. The total pore volume and the pore radius distribution were calculated using the BJH (Barrett-Joyner-Halenda) model at a relative partial pressure of $P/P_0 = 0.95$.

The mechanical strength (kg/cm^2) of the catalysts was studied on a PK-21-2.5 "Catalyst Strength Tester" unit to determine the crush strength of catalyst and sorbent granules under static conditions by the compression method, as per ASTM D6175-03 (2019) "Standard Test Method for Radial Crush Strength of Extruded Catalyst and Catalyst Carrier Particles."

Thermal analysis of the bentonite clays was performed on a Mettler Toledo STARe system under the following conditions: a temperature range of 50-1000°C, a heating rate of 10°C/min, and a sample weight of 100 mg.

The economic efficiency of bentonite as a binder component was evaluated using a process-based costing methodology adapted from a techno-economic analysis of MOF synthesis [34]. In contrast to the full model (CEst = CMat + CMan), the calculation was limited to material costs (CMat), i.e., the cost of reagents. Manufacturing costs, CMan (equipment depreciation, energy, labor), require industrial-scale data and are comparable for all samples since they share a single process route; therefore, these costs do not affect the outcome of the comparison.

The cost of the support was calculated as the sum of the products of each reagent's mass per batch and its price per kilogram, divided by the product yield mass, in $/kg. Prices were taken from the Sigma-Aldrich (Merck KGaA) price list; for items without a listed price, the purchase prices of the reagents were used. The calculation may contain an error, which is insignificant for a relative comparison of the catalysts using a unified methodology. The calculation was performed for MAS:H-bentonite 20/80 and 35/65, and the resulting cost was additionally normalized to the specific surface area (SSA) in $/m2.

3. Results and Discussion

Previous studies [30–33] have investigated the catalytic activity of catalysts supported on a mesoporous aluminosilicate/bentonite mixture (35:65 and 20:80 wt.%) and modified with various metals. The present work focuses on bentonite as the second key component of the support. Its suitability as a binder is determined by its thermal, textural, mechanical, and acidic properties, as well as its cost compared to conventional synthetic binders.

3.1. Phase and chemical composition of bentonite (Western and Eastern Quarries)

Experimental data on the phase composition of bentonite clays from the Western and Eastern quarries of the Tagan field are presented in Table 1. The phase composition was determined by powder X-ray diffraction – the most informative technique for the quantitative determination of clay minerals [35]

Table 1
Phase composition of bentonite clays from the Tagan field

No.	Quarry	Horizon	Phase Composition			Montmorillonite, %	Basal Spacing, Å
			SiO_2	Fe_2O_3	TiO_2		
1	Western	12	2.0	-	-	98.0	8.87
		13	31.0	-	1.0	68.0	9.37
		14	17.7	-	0.5	81.8	9.41
2	Eastern	12	4.2	-	-	96.0	9.70
		13	27.0	8.0	1.0	64.0	9.66
		14	13.8	-	0.5	85.4	9.70

As shown in Table 1, the main rock-forming mineral of the clays under study is montmorillonite, the content of which is largely determined not only by the deposit but also by the depth of the seam. For example, in samples taken from the Western and Eastern quarries, the montmorillonite content for clays from the 12th and 14th horizons ranges from 81.8% to 98.0%, whereas for the sample from the 13th horizon, the montmorillonite content is 20% lower. These samples also differ in their silica gel content. The highest amount is found in the clays of the 13th horizon. It should also be noted that the clay from the 13th horizon in the eastern part of the deposit contains a significant amount of iron oxide (~ 8%). The interlayer spacing value is practically the same for all the clays studied.

The basal spacings d_{001} of all samples lie in a narrow range of 8.87–9.70 Å. By Bragg's rule, the position of the 001 reflection is set by the number and nature of the hydrating interlayer cations [36]: a homogeneously dehydrated Na-montmorillonite gives $d_{001} \approx 9.5–10$ Å (single-layer hydration, small-radius hydration shell of Na^+), whereas Ca-forms yield $d_{001} \approx 12–15$ Å (two-layer hydration) [37,38]. In the present case, the Western horizon 12 (d_{001} = 8.87 Å) shows a slightly "compressed" interlayer, which is consistent with the predominantly Na-cationic composition of this sample, while the Eastern quarry samples (9.66–9.70 Å) all have larger d_{001} values typical of a higher share of Ca^{2+}-form [39]. The close uniformity of d_{001} within a single quarry implies that under acid activation the differences between horizons will be determined less by the layer architecture than by the composition of the exchangeable cations and by the montmorillonite fraction itself.

Finally, phase analysis detects iron oxides only in two samples – 8.0% Fe_2O_3 in horizon 13 of the Eastern quarry and 1.0% in horizon 14 of the Western quarry. This X-ray signal points to the presence of crystalline Fe-bearing phases in the rock (goethite, hematite, or a nontronite-like Fe–montmorillonitic component). However, quantitative phase analysis alone does not provide a complete picture of the rock-forming components and the composition of exchangeable cations — for which reason a chemical analysis was performed (see Table 2).

Table 2
Chemical composition of bentonite clays from the Tagan field

Quarry	Horizon	Content of the main components, % by mass										
		SiO_2	Al_2O_3	Fe_2O_3	TiO_2	CaO	MgO	Na_2O	K_2O	P_2O_5	Mn_2O	LOI
West	12	52.86	19.84	1.05	0.09	0.91	3.18	0.83	0.08	0.01	0.00	20.58
	13	58.85	12.95	6.96	0.83	0.72	2.95	0.50	0.05	0.03	01.0	16.15
	14	56.56	13.95	5.25	0.60	0.70	3.35	0.50	0.04	0.02	0.09	18.93
East	12	50.94	17.95	2.31	0.18	1.52	3.60	0.50	0.07	0.03	0.05	22.90
	13	44.10	19.24	17.84	1.16	1.04	1.68	0.50	0.07	0.11	0.27	24.66
	14	54.10	14.85	4.35	0.51	1.40	3.12	2.64	0.07	0.01	0.09	20.41

** LOI - loss-on-ignition*

The chemical composition of the Tagan clays is dominated by silicon oxide (44.10–58.85%) and aluminum oxide (12.95–19.84%). The distribution of these two components already reveals a non-trivial relation to phase composition: in the Western samples the SiO_2/Al_2O_3 ratio increases as the montmorillonite fraction decreases (2.66 → 4.54 → 4.05 for horizons 12 → 13 → 14), directly reflecting the accumulation of free SiO_2 in horizon 13. This observation reproduces the pattern characteristic of bentonites of volcano-sedimentary origin: the higher the fraction of non-clay SiO_2 in the rock, the higher the Si/Al index [40, 41]. In the Eastern quarry this trend is preserved for horizons 12 and 14 (2.84 and 3.64) but breaks down in horizon 13 — the Si/Al ratio falls to an anomalously low 2.29, the only sample in which the sharp drop in clay content coincides with virtually no reduction in Al_2O_3 (19.24%) and with a drop in SiO_2 to the lowest value in the whole deposit (44.10%). The reason is the abrupt rise in Fe_2O_3 to 17.84%, which points to an Fe-enriched smectite component (of the nontronite series, with Fe^{3+} replacing Al^{3+} in octahedral sites) and/or to an admixture of amorphous Fe-oxyhydroxides not registered by XRD in the phase analysis [42, 43]. This mineralogical "anomaly" of horizon 13 in the Eastern quarry will determine its specific behaviour under acid activation: under H^+ leaching, the dominant contribution to the kinetics will come from Fe rather than from Al.

By the composition of exchangeable cations, the samples from the two quarries belong to different genetic types. In the Western quarry, the elevated Na_2O (0.50–0.83%) and low CaO (0.70–0.91%) and MgO typical for smectites (2.95–3.35%), identify the clay component as alkaline montmorillonite). In the Eastern quarry the markedly higher CaO (1.04–1.52%) together with the Na_2O (0.50–2.64%) and MgO of 1.68–3.60% unambiguously identifies the clay component as Ca-montmorillonite [44]. In both quarries MgO is at its minimum in horizon 13 (2.95% Western, 1.68% Eastern), which may indicate Mg-depleted interlayers and the mobility of Mg^{2+} already under natural conditions. At the same time Fe_2O_3 is at its maximum in the very same horizons 13 (6.96 and 17.84%), so that the rock exhibits a direct octahedral Mg to Fe isomorphism: magnesium is removed from the smectite octahedra, while iron takes its place — a typical pattern of diagenetic transformation of montmorillonite.

The loss-on-ignition (LOI, 16.15–24.66. %) is typical for bentonites and is governed mainly by the release of interlayer water and by dehydroxylation of octahedral OH groups. It correlates markedly with the montmorillonite content (the higher the clay fraction, the more water retained in the structure): Western 12 (98%) — LOI 20.58%; Eastern 12 (96%) — 22.90%. Horizon 13 of the Eastern quarry deviates from this pattern — it has the largest LOI value (24.66%) despite the lowest montmorillonite content (64%), which is explained by the additional release of structural water from Fe-oxyhydroxides.

Such pronounced heterogeneity of the chemical and cation-exchange composition of natural Tagan bentonite — variations of the Si/Al index from 2.29 to 4.54, a switch of the dominant exchangeable-cation type, and the Fe-enrichment anomaly of horizon 13 — necessitates its targeted modification in order to obtain a material with stable and reproducible characteristics. The most common approach to the modification of bentonite clays is acid activation, based on cation exchange in mineral-acid solutions with the formation of the H-form of the aluminosilicate. Treatment of Tagan bentonite with a 20% H_2SO_4 solution (≈ 2–3 M) proceeds in three successive stages — (i) cation exchange and conversion of the framework to the H-form with a decrease in CEC (Cation Exchange Capacity)and the appearance of silanol Si–OH groups, which proceeds more readily for the alkaline montmorillonites of the Western quarry than for the Ca-forms of the Eastern; (ii) selective leaching of octahedral cations in the order $Mg^{2+} > Fe^{3+} > Al^{3+}$, with the tetrahedral SiO_4 groups remaining practically intact and amorphous SiO_2 being accumulated in the interlayer space (in similar Tagan-type bentonites SiO_2 may rise to ~ 74–87%, Al_2O_3 fall to ~ 4.5%, and the Si/Al index increase from ~ 7 to ~ 30); and (iii) textural rearrangement, with a 2.6–3.6-fold increase in specific surface area, the development of mesoporosity, and an increase in mean pore diameter from 50.8 to 92.0 Å. The depth and direction of each stage is set by the mineralogy of the starting sample: for horizon 13 of the Eastern quarry, Fe-leaching dominates; for the Na-bentonites of the Western, easy cation exchange; for the Ca-bentonites, a competition between exchange and leaching, which calls for an individual choice of acid concentration (~ 2 M as an optimum for Ca-forms).

3.2. Acidic properties (NH_3-TPD)

Building on the chemical and cation-exchange data presented above, the next step was to investigate the surface acidity of the materials by temperature-programmed desorption of ammonia (NH_3-TPD). As noted above, the acid activation of Tagan bentonite with sulfuric acid is accompanied by an increase in surface acidity, driven by the replacement of exchangeable cations with hydrogen ions and by the formation of new acid sites. The acidic properties of the MAS support were examined in detail in our previous works [30–33]; in the present study, these results are provided only for a clear comparison with the composite support based on H-bentonite. The NH_3-TPD profiles of the samples investigated are shown in Fig. 2, and the corresponding quantitative characteristics are given in Table 3.

Table 3
Concentration and strength of acid sites for MA, H-bentonite and MAS-H-bentonite

№	Sample	Number of acid sites (amount of adsorbed NH_3, μmol/g)			
		Weak T_{max} < 300°C	Medium T_{max} = 300–500°C	Strong T_{max} > 500°C	Total
1.	MAS	1144	27	–	1171
2.	H-bentonite	4819	18	–	4837
3.	MAS- H-bentonite	1193	–	–	1193

According to the data in Fig. 2 and Table 3, the ammonia desorption curves for the samples of mesoporous aluminosilicate, pre-activated bentonite, and the composite based on them all have a similar shape, each exhibiting a single thermodesorption peak. However, these samples differ in the strength and concentration of their acid sites. For instance, the synthesized mesoporous aluminosilicate sample has approximately 98% weak acid sites (1144 μmol/g) and 2% medium-strength acid sites (27 μmol/g), whereas for pre-activated bentonite, the concentration of weak acid sites is almost four times higher, at 4819 μmol/g. Mixing mesoporous aluminosilicate with activated bentonite causes the ammonia desorption peak to shift toward higher temperatures compared to the activated bentonite sample, which indicates an increase in the strength of the acid sites. However, the area under the ammonia desorption curve decreases.

The high acidity of H-bentonite is consistent with literature data, which states that the acid activation of montmorillonite with sulfuric acid leads to the formation of additional acid sites due to the leaching of octahedral cations and partial dealumination of the structure [45, 46]. The results obtained indicate that introducing H-bentonite into the composite changes the distribution of acid sites, forming fewer but stronger acid sites, which may enhance the catalytic activity of the material.

3.3. Textural properties of the composite

Alongside surface acidity, the texture of porous supports plays a key role in their performance: the extent of the specific surface area, the pore volume, and the pore size distribution directly determine how accessible the active sites are to reactant molecules and how freely these molecules can move within the material's structure. The textural properties of the synthesized samples were characterized by low-temperature nitrogen adsorption–desorption. The resulting values of specific surface area, pore volume, and average pore diameter are summarized in Table 4.

Table 4
Physical properties of the samples

№	Catalyst	SSA, m^2/g	Pore volume, cm^3/g	Average pore diameter, nm
1.	MAS-2 (uncalcined)	291.8	0.4158	1.933
2.	MAS-2 (calcined)	511.0	1.469	3.82
3.	MAS-2/H-bentonite	375.1	0.3523	3.5

Thermal removal of the structure-directing template upon calcination of the mesoporous aluminosilicate is accompanied by a pronounced reorganization of its textural characteristics (Table 4): the specific surface area increases 1.75-fold (from 291.8 to 511.0 m^2/g), the pore volume increases 3.5-fold (from 0.4158 to 1.469 cm^3/g), and the average pore diameter nearly doubles (from 1.93 to 3.82 nm). Such a pronounced enhancement of the textural parameters is consistent with the template-directed mechanism of mesoporous material formation: in the dried sample, the pore space of the framework remains partially occupied by surfactant molecules, and only their thermal decomposition and removal during calcination liberates the channel system, giving rise to a well-developed, topologically connected mesoporous structure.

Incorporation of H-bentonite into the support (35 wt. %) exerts an opposite, yet substantially less pronounced, effect: the specific surface area and pore volume of the composite decrease to 375.1 m^2/g and 0.3523 cm^3/g, respectively, occupying an intermediate position between the uncalcined and calcined MAS. Notably, the average pore diameter changes only marginally (3.5 nm versus 3.82

nm for pure calcined MAS), indicating that the mesoporous architecture of the framework is essentially preserved. The observed decrease in SSA and pore volume is therefore attributable not to structural degradation or pore narrowing, but rather to the inherently lower intrinsic porosity of the bentonite phase and to partial screening of a fraction of the mesopores by clay particles incorporated during composite formation. Thus, the introduction of bentonite results in a moderate — rather than deleterious — reduction of the textural characteristics of the support, whereby the functionally relevant mesoporous nature of the material remains intact, consistent with the objective of simultaneously reducing cost while preserving the operational properties of the catalyst system.

3.4. Mechanical strength and bulk density

The mechanical strength of catalyst granules is one of the key factors determining the reliability and operational efficiency of a reactor under industrial conditions [47]. Insufficient strength leads to granule breakdown under the weight of the bed itself, the flow of the reaction mixture, and thermal fluctuations, resulting in the formation of fines and dust. This, in turn, causes an increase in the hydraulic resistance of the bed, uneven flow distribution, and localized overheating, as well as accelerated loss of the active phase — collectively, these factors significantly shorten the between-regeneration run length and the overall service life of the catalyst. In this regard, the physicomechanical characteristics of the synthesized samples were determined, and the results are presented in Table 5.

Table 5
Bulk density and mechanical strength of catalysts

Catalyst	Bulk density, g/cm^3	Mechanical strength, kg/cm^2
MAS-2	0.478	27.1
MAS-H-bentonite	0.424	30.2

The introduction of H-bentonite into the composite support results in a simultaneous and, at first glance, counterintuitive change in its physico-mechanical properties (Table 5): the crushing strength of the granules increases from 27.1 to 30.2 kg/cm² (an 11.4% improvement), while the bulk density decreases from 0.478 to 0.424 g/cm³. Conventionally, higher packing density is expected to correlate positively with mechanical strength, so the concurrent rise in strength and decline in density observed here warrants closer examination.

A comparable inverse relationship between bulk density and compressive strength has been reported for other bentonite-containing composite systems, where scanning electron microscopy revealed that the incorporation of bentonite homogenizes the pore-size distribution throughout the material's cross-section — pores of more uniform size and distribution promote a more even distribution of mechanical stress across the microstructure, thereby increasing resistance to crushing even as the overall density of the material decreases [48]. This mechanism is consistent with the textural data presented in Table 4, where the introduction of H-bentonite was shown to reduce the specific surface area and pore volume of the composite while leaving the average pore diameter virtually unchanged (3.5 nm), indicating that the mesoporous framework is not destroyed but rather structurally redistributed upon composite formation. Taken together, these observations suggest that the strength enhancement observed for the MAS-H-bentonite composite arises not from denser particle packing, but from a more homogeneous internal pore architecture that reduces stress-concentration points within individual granules.

Notably, the resulting bulk density of 0.424 g/cm³, while lower than the 0.8–1.2 g/cm³ range typically reported for industrially optimized fixed-bed catalysts in refining and synthesis applications, remains consistent with values expected for laboratory-scale porous aluminosilicate supports prior to industrial-scale densification optimization [49]. Given that catalyst loading technology explicitly links packing density to particle integrity and pressure-drop behavior in fixed-bed operation], the observed increase in crushing strength accompanying the density reduction represents a favorable combination for practical reactor loading, rather than a trade-off requiring further optimization. Taken together, the results in Table 5 demonstrate that partial replacement of MAS with H-bentonite yields a mechanically more robust catalyst support without introducing physical limitations for its intended application, reinforcing the broader conclusion that bentonite functions not merely as an inert diluent, but as a structurally active component that measurably improves the granule integrity of the composite catalyst.

3.5. Thermal behavior

To evaluate the thermal behavior of the bentonite clays, differential thermal analysis (DTA) was performed. The DTA curves of the bentonite samples from the Eastern and Western quarries of the Tagan field are presented in Figs. 3 and 4.

All investigated samples exhibit a similar sequence of thermal effects, indicating a common mineralogical nature. The first endothermic effect is observed in the low-temperature region (approximately 60–190°C) and is associated with the removal of physically adsorbed and interlayer water. A pronounced thermal effect is then observed at approximately 265°C, followed by another endothermic effect centered at about 455°C, reflecting further structural transformations of the clay minerals.

The main differences between the samples appear in the high-temperature region. Curve 2 exhibits additional thermal effects at approximately 530, 660, and 870°C, whereas curves 1 and 3 are characterized by a single pronounced endothermic effect near 905°C. These differences indicate variations in the mineral composition of the samples and most likely reflect different amounts of accessory mineral phases rather than changes in the dominant clay mineral. It should be noted that bentonite clays are characterized by a lower melting point compared to kaolinite clays, which is due to the peculiarities of their layered structure and chemical composition.

Tagan field

A comparison of the DTA curves for the Eastern and Western quarry samples shows that the positions of the main thermal effects are nearly identical, while their intensity and the number of high-temperature effects vary slightly. Similar behavior has been reported for natural bentonites and smectite-rich clays, where differences in the high-temperature region are attributed to variations in exchangeable cations, crystallinity, and the presence of quartz, feldspars, carbonates, or other accessory minerals, rather than to changes in the primary montmorillonite phase [50].

Overall, the DTA results confirm that the investigated bentonite samples possess similar thermal characteristics typical of montmorillonite-rich clays. The observed differences between individual samples are mainly associated with variations in the content of accompanying mineral phases and do not affect the overall thermal behavior of the material.

3.6. Cost-effectiveness of bentonite as a binder component

The vast majority of research on catalysts based on mesoporous aluminosilicates focuses on improving their textural, acidic, and catalytic properties, while the cost of raw materials and synthesis remains largely unexplored. However, it is the cost of the support that ultimately determines the real prospect of scaling a catalyst from laboratory synthesis to industrial application. In this work, the economic feasibility of introducing bentonite into the support composition was evaluated by calculating reagent costs based on prices from official sources: Sigma-Aldrich (Merck KGaA) and TAGBENT LLP (Tagan field). When a reagent price was given per liter, it was recalculated to the cost per kilogram using the density specified in the corresponding reagent description on the Sigma-Aldrich website. The batch cost was then converted to the cost per kilogram of the finished support (see Table 6).

Table 6

Calculation of the cost-effectiveness of bentonite (K1–K6)

Cost Calculation for Catalysts K1–K6

									EUR/USD rate	1,15	[51]	
									KZT/USD rate	475,00	[52]	
Catalyst	Synthesis stage	Reagent	Amount (original unit)	Unit	Density (for conversion to g)	Unit	Amount, g	Amount, kg	Price, EUR/kg (if quoted per liter, converted to per kg)	Price, $/kg	Cost per batch, $	Source
K1	MAS-2, pure (no bentonite)											
	1. Alkoxide dissolution	aluminum sec-butoxide (sec-BuO)3Al	2,46	g	—	—	2,46	0,00	209,00	239,20	0,59	[53]
	1. Alkoxide dissolution	isopropanol	35,00	mL	0,79	g/mL	27,68	0,03	85,35	98,15	2,70	[54]
	2. TEOS addition	TEOS	22,33	mL	0,94	g/mL	20,9802	0,0209802	96,38	110,84	2,33	[55]
	3. Water addition	distilled water	40,00	mL	1,00	g/mL	40,00	0,04	0,00	0,00	0,00	
	4. Surfactant dissolution	hexadecylamine	6,03	g	—	—	6,03	0,01	157,8	181,47	1,09	[56]
	4. Surfactant dissolution	isopropanol	28,50	mL	0,79	g/mL	22,37	0,02	85,35	98,15	2,20	
	5. Water addition to surfactant	distilled water	100,00	mL	1,00	g/mL	100,00	0,10	0,00	0,00	0,00	
	6. Combining solutions + water	distilled water	40,00	mL	1,00	g/mL	40,00	0,04	0,00	0,00	0,00	
										TOTAL PER BATCH →	8,90	Price per kg: $1935.18
K2	MAS-1, pure (no bentonite)											
	1. Alkoxide dissolution	aluminum isopropoxide Al(O-i-Pr)3	2,46	g	—	—	2,46	0,00	77,30	88,90	0,22	[57]
	1. Alkoxide dissolution	isopropanol	35,00	mL	0,79	g/mL	27,68	0,03	85,35	98,15	2,70	
	2. TEOS addition	TEOS	22,33	mL	0,94	g/mL	20,93	0,02	96,38	110,84	2,31	
	3. Water addition	distilled water	40,00	mL	1,00	g/mL	40,00	0,04	0,00	0,00	0,00	
	4. Surfactant dissolution	hexadecylamine	6,03	g	—	—	6,03	0,01	157,8	181,47	1,09	
	4. Surfactant dissolution	isopropanol	28,50	mL	0,79	g/mL	22,37	0,02	85,35	98,15	2,20	
	5. Water addition to surfactant	distilled water	100,00	mL	1,00	g/mL	100,00	0,10	0,00	0,00	0,00	
	6. Combining solutions + water	distilled water	40,00	mL	1,00	g/mL	40,00	0,04	0,00	0,00	0,00	
										TOTAL PER BATCH →	8,81	Price per kg: $1892.18
K3	MAS-2-H-bentonite, 20/80											
	1. MAS component (recipe share, 100 g basis)	MAS (batch share)	20,00	g	—	—	20,00	0,02	—	1935,18	38,70	
	2. Bentonite activation (10 g:150 mL 20% H2SO4)	Raw bentonite (Tagan field)	80,00	g	—	—	80,00	0,08	—	0,12	0,01	[58]
	2. Bentonite activation (10 g:150 mL 20% H2SO4)	H2SO4, 20% solution	1200,00	mL	1,14	g/mL	1368,00	1,37	13,65 (recalculated for 28% solution)	15,6975	21,47	[59]
										TOTAL PER BATCH →	60,19	
K4	MAS-2-H-bentonite, 35/65											
	1. MAS component (recipe share, 100 g basis)	MAS (batch share)	35,00	g	—	—	35,00	0,04	—	1935,18	67,73	
	2. Bentonite activation (10 g:150 mL 20% H2SO4)	Raw bentonite (Tagan field)	65,00	g	—	—	65,00	0,07	—	0,12	0,01	
	2. Bentonite activation (10 g:150 mL 20% H2SO4)	H2SO4, 20% solution	975,00	mL	1,14	g/mL	1111,50	1,11	13,65 (recalculated for 28% solution)	15,6975	17,45	
										TOTAL PER BATCH →	85,19	
K5	MAS-1-H-bentonite, 20/80											
	1. MAS component (recipe share, 100 g basis)	MAS (batch share)	20,00	g	—	—	20,00	0,02	—	1892,18	37,84	
	2. Bentonite activation (10 g:150 mL 20% H2SO4)	Raw bentonite (Tagan field)	80,00	g	—	—	80,00	0,08	—	0,12	0,01	
	2. Bentonite activation (10 g:150 mL 20% H2SO4)	H2SO4, 20% solution	1200,00	mL	1,14	g/mL	1368,00	1,37	13,65 (recalculated for 28% solution)	15,6975	21,47	
										TOTAL PER BATCH →	59,33	
K6	MAS-1-H-bentonite, 35/65											
	1. MAS component (recipe share, 100 g basis)	MAS (batch share)	35,00	g	—	—	35,00	0,04	—	1892,18	66,23	—
	2. Bentonite activation (10 g:150 mL 20% H2SO4)	Raw bentonite (Tagan field)	65,00	g	—	—	65,00	0,07	—	0,12	0,01	—
	2. Bentonite activation (10 g:150 mL 20% H2SO4)	H2SO4, 20% solution	975,00	mL	1,14	g/mL	1111,50	1,11	13,65 (recalculated for 28% solution)	15,6975	17,45	—
										TOTAL PER BATCH →	83,68	

SUMMARY: cost and normalization to specific surface area (SSA)

Catalyst	Total feedstock, $	Yield / basis, g	Yield, kg	Price, $/kg
K1	8,90	4,6	0,0	1935,18
K2	8,81	4,5	0,0	1892,18
K3	60,19	100	0	601,87
K4	85,19	100	0	851,87
K5	59,33	100	0	593,27
K6	83,68	100	0	836,82

The introduction of bentonite into the support composition leads to a pronounced and predictable decrease in its cost. The cost of the initial MAS-1 and MAS-2 is $1935/kg and $1892/kg for samples based on sec-butoxide and isopropoxide aluminum precursors, respectively—meaning the choice of aluminum source has practically no effect on the cost of the pure support component. When part of the MAS is replaced with bentonite in a 20:80 ratio, the cost is reduced by 69%, and at a 35:65 ratio, by 56%. This demonstrates a direct correlation between the economic effect and the mass fraction of the binder in the composite, similar to how in the techno-economic analysis of metal-organic framework synthesis [34], reducing the proportion of the system's expensive component (the organic solvent) served as the primary lever for lowering the cost of the final material.

The presented estimates are based on retail prices of reagents and do not include manufacturing costs; therefore, the absolute values should be considered approximate. However, since all compositions were evaluated using a single methodology, the relative comparison between them remains a reliable basis for selecting the most economically favorable component ratio.

4. Conclusions

The results of this work confirm the role of bentonite as a low-cost binder component in mesoporous aluminosilicate composites.

Bentonite from the Western and Eastern quarries of the Tagan field is characterized by a high montmorillonite content (81.8–98.0 wt. % for horizons 12 and 14). However, the composition of exchangeable cations varies across different sections of the deposit, which necessitates acid activation to obtain a material with stable characteristics. Activation with H_2SO_4 increases the concentration of weak acid sites almost fourfold compared to pure MAS (4819 versus 1144 μmol/g), while the introduction of H-bentonite into the composite redistributes the acid sites, forming fewer of them but with a greater binding strength.

The introduction of H-bentonite (35 wt. %) reduces the specific surface area of the support from 511.0 to 375.1 m^2/g and the pore volume to 0.3523 cm^3/g, while the average pore diameter is maintained at 3.5 nm, indicating that the mesoporous structure is not destroyed. Simultaneously, the mechanical strength of the granules increases from 27.1 to 30.2 kg/cm^2, while the bulk density decreases from 0.478 to 0.424 g/cm^3.

An economic assessment showed that the cost of unmodified MAS is $1892–1935/kg, regardless of the nature of the aluminum precursor, whereas replacing part of it with bentonite reduces the support's cost by 69% at a MAS:bentonite ratio of 20:80 and by 56% at a ratio of 35:65.

Thus, bentonite from the Tagan deposit provides a significant reduction in the cost of the carrier while maintaining its textural and mechanical functionality. This confirms the feasibility of its use as a stable and cost-effective alternative to synthetic binders in catalyst systems.

Declarations

Author Contributions: Conceptualization, K. U., G.V.; methodology, K. U., T.A.; software, F.K; validation, S.A., M.S. and A.A.; formal analysis, K.U., D.B.; investigation, K.U., G.V., D.B.; resources, K.U., G.V.; data curation, S.A.; writing—original draft preparation, K.U., M.S., F.K.; writing—review and editing, G.V., T.A.; visualization, D.B.; supervision, G.V.; project administration, K.U., G.V.; funding acquisition, K.U., G.V. All authors have read and agreed to the published version of the manuscript.

Funding: -

Institutional Review Board Statement: Not applicable.

Informed Consent Statement: Not applicable.

Data Availability Statement: The data supporting the findings of this study are available within the article and its Supplementary Information. Additional data are available from the corresponding author upon reasonable request.

Acknowledgments: -

Conflicts of Interest: The authors declare no conflicts of interest.

References

1. Panasyugin, A. S., Tsyganov, A. R. & Masherova, N. P. Preface in *Modified Bentonite Clays as Sorbents, Catalysts, and Active Catalytic Phase Carriers* (eds Leshchev, S. M. & Smorygo, O. L.) 3 (Belarusian State Technological University, 2022).
2. Vasilyanova, L. S. Bentonites in ecology. *Sci. News Kazakhstan* 3, 70-101 (2016).
3. Uddin, F. Clays, nanoclays, and montmorillonite minerals. *Metall. Mater. Trans. A* 39, 2804-2814; 10.1007/s11661-008-9603-5 (2008).
4. Luo, Y. *et al.* Synthesis of pillared nanoporous bentonite as potential solid acid catalyst for catalysis of Friedel-Crafts alkylation of diphenylamine with diisobutylene. *Inorg. Chem. Commun.* 191, 117009; 10.1016/j.inoche.2026.117009 (2026).
5. Baş, İ. *et al.* Mineralogy, geochemistry and genesis of K-bentonites in Early-Middle Jurassic volcano-sedimentary sequences from NE Türkiye. *J. Afr. Earth Sci.* 241, 106205; 10.1016/j.jafrearsci.2026.106205 (2026).
6. Saad, I. *et al.* Physico-mechanical reinforcement and antimicrobial efficiency of green-synthesized Ca/exfoliated bentonite/chitosan nanocomposites. *Beni-Suef Univ. J. Basic Appl. Sci.* 15, 8; 10.1186/s43088-025-00725-8 (2026).

7. Rubtsova, M. *et al.* Mesoporogen-free SAPO-11/halloysite catalysts: bridging cost-effective synthesis and high-performance in hydroisomerization of n-hexadecane. *Fuel* 427, 139654; 10.1016/j.fuel.2026.139654 (2027).
8. Bergaya, F. & Lagaly, G. Surface modification of clay minerals. Appl. Clay Sci. 19, 1-3; 10.1016/S0169-1317(01)00063-1 (2001).
9. Steudel, A. Selection Strategy and Modification of Layer Silicates for Technical Application 278 (Universität Karlsruhe, 2010).
10. Trofimova, F. A., Lygina, T. Z. & Naumkina, N. N. et al. Structural changes of bentonite-containing clays during modification in Structure and Dynamics of Molecular Systems 301-305 (2006).
11. Oster, J. D., Shainberg, I. & Wood, J. D. Flocculation value and gel structure of sodium/calcium montmorillonite and illite suspensions. Soil Sci. Soc. Am. J. 44, 955-959; 10.2136/sssaj1980.03615995004400050016x (1980).
12. Dehshiri, E. et al. Impact of filter cake water chemistry on bentonite functionality and pellet quality in magnetite pelletizing. Mater. Chem. Phys. 363, 132773; 10.1016/j.matchemphys.2026.132773 (2026).
13. Komadel, P. & Madejová, J. Acid activation of clay minerals in Handbook of Clay Science Vol. 1 263-287; 10.1016/S1572-4352(05)01008-1 (2006).
14. Öz, M. et al. Application and performance of bentonite–leonardite mixture for feed-derived nitrogen removal in freshwater aquaculture systems. Sci. Rep. 16, 19372 (2026).
15. Noghretab, B. S. et al. 3D coupled multiphase flow and hydromechanical modeling of an MX-80 bentonite pellet/powder mixture. Appl. Clay Sci. 290, 108239; 10.1016/j.clay.2026.108239 (2026).
16. Zereffa, E. A. et al. Phyto-mediated synthesis of ZnO/TiO2/bentonite nanocomposites. Sci. Rep. 16 (2026).
17. Benabadji, K. I. et al. In-situ polymerization of (acrylamide/bisacrylamide)/bentonite composites and their application for dye removal. Phys. Chem. Res. 14, 29-42 (2026).
18. Lee, C.-P. & Tsai, S.-C. Colloid stability and radionuclide adsorption on bentonite colloids: relevance to conservative safety assessment assumptions. Nucl. Eng. Technol. 58, 104499; 10.1016/j.net.2026.104499 (2026).
19. Xu, X. et al. The temperature dependence of bentonite's thermal conductivity and its influence on the temperature distributions in deep geological repositories. Int. Commun. Heat Mass Transf. 178, 111621; 10.1016/j.icheatmasstransfer.2026.111621 (2026).
20. Liu, H., Xie, B. & Qin, Y.-L. Effect of bentonite on the pelleting properties of iron concentrate. *J. Chem.* 2017, 7639326; 10.1155/2017/7639326 (2017).
21. Xu, R. et al. Development of pillared modified bentonite catalysts for catalysis of Friedel-Crafts alkylation of diphenylamine with nonene. Mater. Lett. 414, 140547; 10.1016/j.matlet.2026.140547 (2026).
22. Boyjanov, N. I. et al. Mathematical analysis of the linear increase in SiO2 content during the activation of Navbakhor alkaline bentonite with hydrochloric acid. Complex Use Miner. Resour. 342, 90-99 (2027).
23. Hamza, W., Chtara, C. & Benzina, M. Characterization and application of Fe and iso-Ti-pillared bentonite on retention of organic matter contained in wet industrial phosphoric acid (54%). Res. Chem. Intermed. 41, 6117-6140 (2015).
24. Kadeche, A. et al. Preparation, characterization and application of Fe-pillared bentonite to the removal of Coomassie blue dye from aqueous solution. Res. Chem. Intermed. 46, 4985-5008 (2020).
25. Slimani, M. S., Aazza, M. & Ahlafi, H. et al. Adsorptive removal of phenolic compounds from olive mill wastewater by Na+-bentonite and HDTMA+-modified bentonite. J. Mol. Liq. 457, 129704; 10.1016/j.molliq.2026.129704 (2026).
26. Emad, G., Elgamal, A. & Ashoor, N. M. Sustainable green concrete: multicriteria optimization of bentonite–fly ash–silica fume ternary systems. Sci. Rep. 16, 19641 (2026).
27. Mineral Commodity Summaries 2026. Available online: https://pubs.usgs.gov/publication/mcs2026, https://pubs.usgs.gov/periodicals/mcs2026/mcs2026-clays.pdf (accessed on 06/08/2026)
28. Data on the volume of bentonite production from the Bureau of National Statistics of the Agency for Strategic Planning and Reforms of the Republic of Kazakhstan. Available online: https://taldau.stat.gov.kz/ru/NewIndex/GetIndex/701608?keyword=бентонит (accessed on 06/08/2026)
29. Resolution of the Government of the Republic of Kazakhstan No. 549 dated July 21, 2025, On approval of the Concept for the development of the oil refining industry of the Republic of Kazakhstan for 2025-2040. Available online: https://adilet.zan.kz/rus/docs/P2500000549 (accessed on 06/08/2026)
30. Vassilina, G., Abdildina, K. & Abdrassilova, A. The influence of feed space velocity and pressure on the cold flow properties of diesel fuel. Open Chem. 23, 20250181 (2025).

31. Vassilina, G., Abdildina, K., Abdrassilova, A. et al. The mesoporous aluminosilicate application as support for bifunctional catalysts for n-hexadecane hydroconversion. Open Chem. 20, 225-236 (2022).
32. Abdildina, K. M., Vassilina, G. K., Abdrassilova, A. K., Klassen, I. A., Orynbassar, R. & Kanapiyeva, F. M. The role of catalyst promotive additives and temperature in the hydroisodewaxing process. Molecules 28, 7598; 10.3390/molecules28227598 (2023).
33. Vassilina, G., Umbetkaliyeva, K., Oktar, N., Karaman, B. P. & Vassilina, T. Characterization and catalytic activity of Ni/mesoporous aluminosilicate HMS and Mo/mesoporous aluminosilicate HMS in the conversion of n-hexadecane. Mater. Today Proc. 10.1016/j.matpr.2020.06.562 (2020).
34. DeSantis, D., Mason, J. A., James, B. D., Houchins, C., Long, J. R. & Veenstra, M. Techno-economic analysis of metal–organic frameworks for hydrogen and natural gas storage. Energy Fuels 31, 2024-2032; 10.1021/acs.energyfuels.6b02510 (2017).
35. Belousov, P. E., Krupskaya, V. V., Zakusin, S. V. & Zhigarev, V. V. Bentonite clays from the 10th Khutor deposit (Republic of Khakassia): features of genesis, composition and adsorption properties. RUDN J. Eng. Res. 18, 135-143; 10.22363/2312-8143-2017-18-1-135-143 (2017).
36. He, Z., Nie, W., Yang, H., Tang, Y., Sha, A., Qu, J., Xu, Z. & Chi, R. Effects of cations on rare earth adsorption and desorption in binding sites of montmorillonite. *Physicochem. Probl. Miner. Process.* 59, 168280; 10.37190/ppmp/168280 (2023).
37. Zhang, X., Yi, H., Bai, H., Zhao, Y., Min, F. & Song, S. Correlation of montmorillonite exfoliation with interlayer cations in the preparation of two-dimensional nanosheets. *RSC Adv.* 7, 41471-41478; 10.1039/c7ra07816a (2017).
38. Parolo, M. E., Avena, M. J., Pettinari, G. R. & Baschini, M. T. Influence of Ca2+ on tetracycline adsorption on montmorillonite. *J. Colloid Interface Sci.* 368, 420-426; 10.1016/j.jcis.2011.10.079 (2012).
39. Perassi, I. & Borgnino, L. Adsorption and surface precipitation of phosphate onto CaCO3–montmorillonite: effect of pH, ionic strength and competition with humic acid. *Geoderma* 232, 600-608; 10.1016/j.geoderma.2014.06.017 (2014).
40. Costafreda Mustelier, J. L., Sánchez Martín, D. A., Sanjuán Barbudo, M. Á. & Costafreda Velázquez, J. L.Bentonite clays from Southeastern Spain as sustainable natural materials for the improvement of cements, mortars and concretes. *Sustainability* 15, 16710; 10.3390/su152416710 (2023).
41. Crespo, E., Martín, D. A. & Costafreda, J. L. Bentonite clays related to volcanosedimentary formations in Southeastern Spain: mineralogical, chemical and pozzolanic characteristics. *Minerals* 14, 814; 10.3390/min14080814 (2024).
42. Babahoum, N. & Ould Hamou, M. Characterization and purification of Algerian natural bentonite for pharmaceutical and cosmetic applications. *BMC Chem.* 15, 50; 10.1186/s13065-021-00776-9 (2021).
43. Yilmaz, G. The effects of temperature on the characteristics of kaolinite and bentonite. *Sci. Res. Essays* 6, 1928-1939; 10.5897/SRE10.727 (2011).
44. Bourliva, A., Michailidis, K., Sikalidis, C. & Filippidis, A. Spectroscopic and thermal study of bentonites from Milos Island, Greece. *Bull. Geol. Soc. Greece* 47, 2020-2029; 10.12681/bgsg.11030 (2013).
45. Huang, W. J., Liu, J. H., She, Q. M., Zhong, J. Q., Christidis, G. E. & Zhou, C. H. Recent advances in engineering montmorillonite into catalysts and related catalysis. *Catal. Rev.* 65, 929-985; 10.1080/01614940.2021.1995163 (2023).
46. Vrbková, E., Stoupová, L. & Vyskočilová, E. Montmorillonite—eco-friendly and effective catalyst in the synthesis of biologically active compounds with bicyclo[3.3.1] moiety. *ACS Omega* 10, 63597-63607; 10.1021/acsomega.5c10876 (2025).
47. Wu, D., Zhou, J. & Li, Y. Mechanical strength of solid catalysts: recent developments and future prospects. *AIChE J.* 53, 2618-2629; 10.1002/aic.11291 (2007).
48. Abdelfattah, M. M., Géber, R., Abdel-Kader, N. A. & Kocserha, I. Assessment of the mineral phase and properties of clay-Ca bentonite lightweight aggregates. *Arab. J. Geosci.* 15, 205; 10.1007/s12517-022-09538-w (2022).
49. Xu, Z., Liu, W., Yin, H. & Liu, X. Catalyst loading technology for fixed-bed reactors: from empirical heuristics to data-driven intelligent regulation. *Catalysts* 16, 123; 10.3390/catal16020123 (2026).
50. Holtzer, M., Bobrowski, A. & Żymankowska-Kumon, S. Temperature influence on structural changes of foundry bentonites. *J. Mol. Struct.* 1004, 102; 10.1016/j.molstruc.2011.07.040 (2011).
51. European Central Bank. Euro foreign exchange reference rates. *European Central Bank*https://www.ecb.europa.eu/stats/policy_and_exchange_rates/euro_reference_exchange_rates/html/index.en.html(accessed 6 August 2026).

52. National Bank of the Republic of Kazakhstan. Official exchange rates. *National Bank of the Republic of Kazakhstan*https://nationalbank.kz/en/exchangerates/ezhednevnye-oficialnye-rynochnye-kursy-valyut (accessed 6 August 2026).
53. Sigma-Aldrich. Aluminum-tri-sec-butoxide, 97%. *Sigma-Aldrich*https://www.sigmaaldrich.com/KZ/en/product/aldrich/201073 (accessed 6 August 2026).
54. Sigma-Aldrich. 2-Propanol, ACS reagent. *Sigma-Aldrich* https://www.sigmaaldrich.com/KZ/en/product/sigald/190764(accessed 6 August 2026).
55. Sigma-Aldrich. Tetraethyl orthosilicate. *Sigma-Aldrich* https://www.sigmaaldrich.com/KZ/en/product/mm/800658(accessed 6 August 2026).
56. Sigma-Aldrich. Hexadecylamine, technical, 90%. *Sigma-Aldrich*https://www.sigmaaldrich.com/KZ/en/product/aldrich/h7408 (accessed 6 August 2026).
57. Sigma-Aldrich. Aluminum isopropoxide, ≥98%. *Sigma-Aldrich*https://www.sigmaaldrich.com/KZ/en/product/aldrich/220418 (accessed 6 August 2026).
58. TAGBENT LLP. Price list. *TAGBENT* https://tagbent.com/price (accessed 6 August 2026).
59. Sigma-Aldrich. Sulfuric acid, ACS reagent, 95.0–98.0%. *Sigma-Aldrich*https://www.sigmaaldrich.com/US/en/product/sigald/258105 (accessed 6 August 2026).

Figures

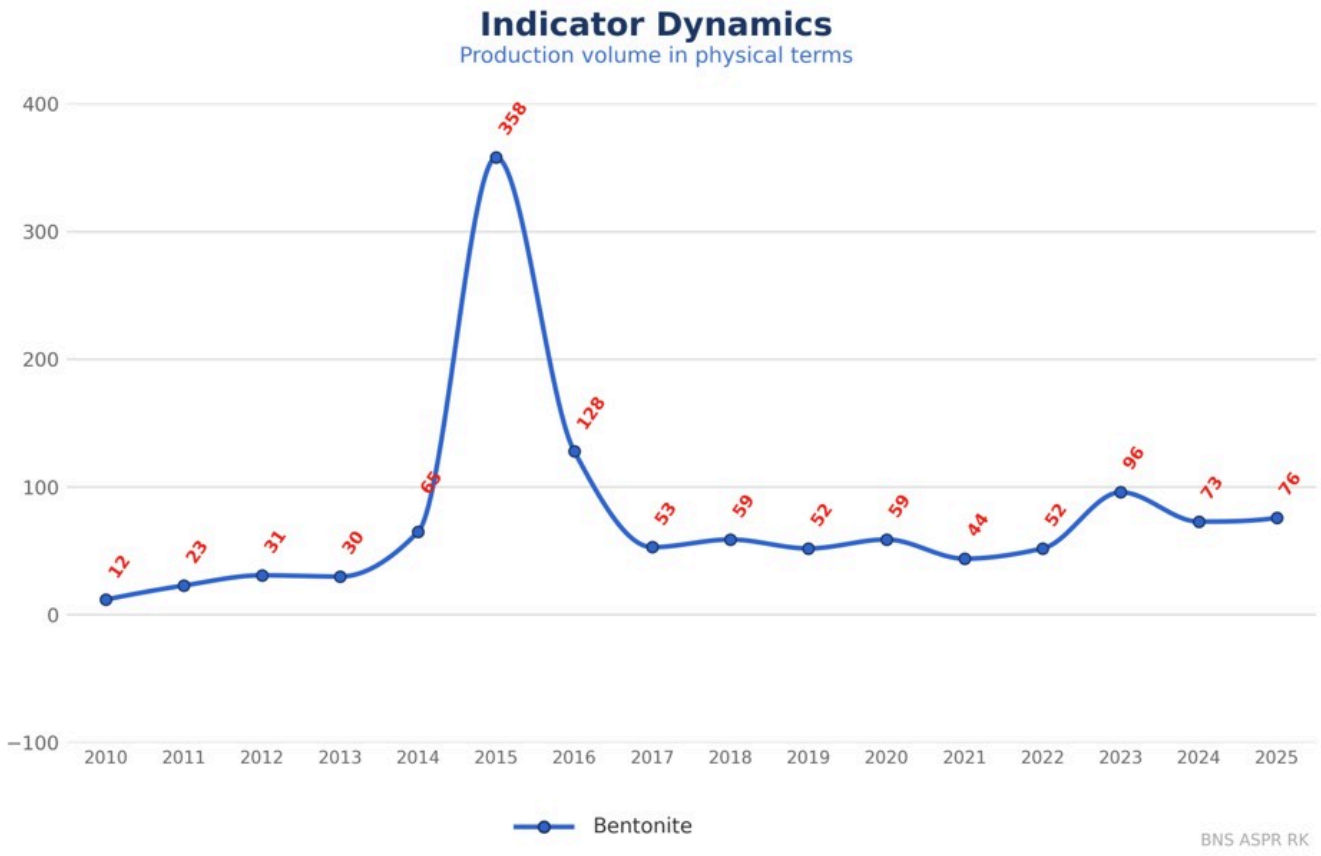


Figure 1

Bentonite production in the Republic of Kazakhstan, 2010–2025, thousand tons

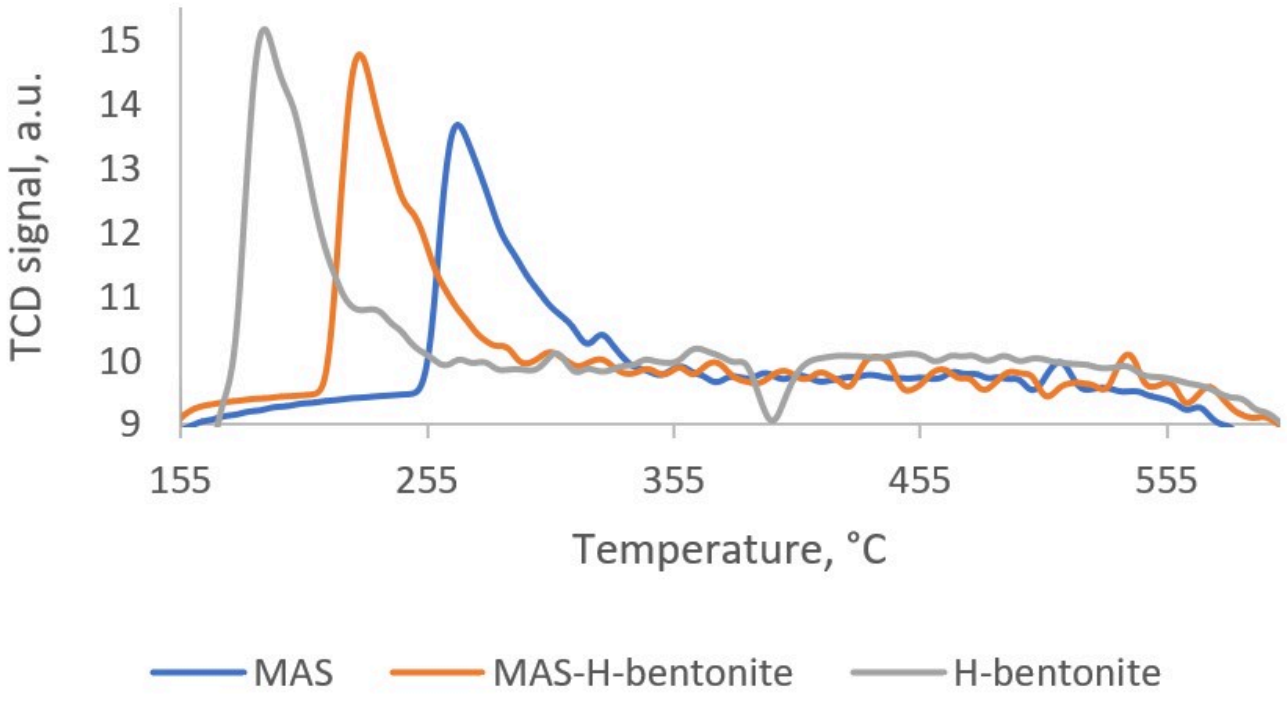


Figure 2

NH_3-TPD curves of mesoporous aluminosilicate, pre-activated bentonite, and an unpromoted composite based on mesoporous aluminosilicate

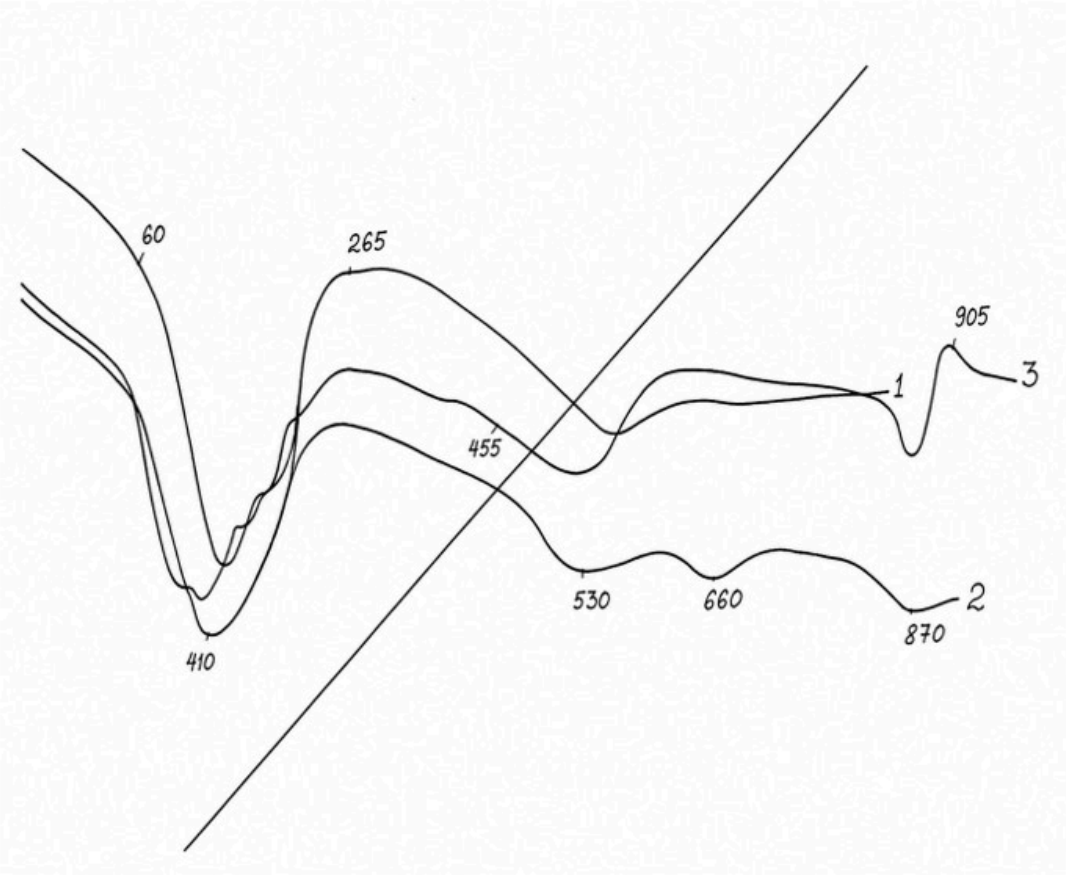


Figure 3

Derivatogram of the initial bentonite clay from the Eastern quarry of the Tagan field

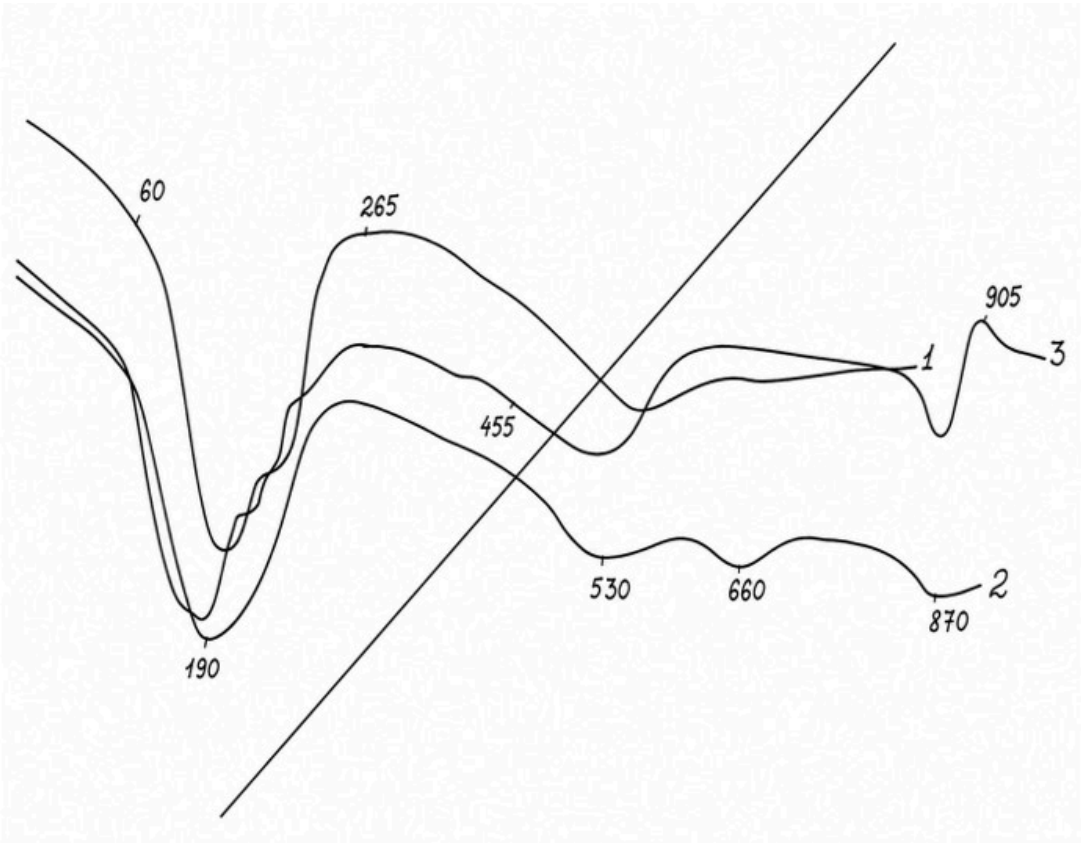


Figure 4

Derivatogram of the initial bentonite clay from the Western quarry of the Tagan field

Supplementary Files

This is a list of supplementary files associated with this preprint. Click to download.

- Catalystostalculation.xlsx
- TPDNH3.xlsx